Journal of Science and Transport Technology
Journal homepage: https://jstt.vn/index.php/en

Nonlinear buckling and postbuckling responses of sandwich cylindrical panels with layered corrugated FG-GRC core resting on elastic foundation

Nguyen Thanh Trung[1], Vu Minh Duc[2,3,*], Vu Tho Hung[4]
[1]Faculty of Civil Engineering, Lac Hong University, Dong Nai, Vietnam
[2]Mechanics of Advanced Materials and Structures, Institute for Advanced Study in Technology, Ton Duc Thang University, Ho Chi Minh City, Vietnam
[3]Faculty of Civil Engineering, Ton Duc Thang University, Ho Chi Minh City, Vietnam
[4]Mechanics of Advanced Materials and Structures, University of Transport Technology, Hanoi, Vietnam

Article info
Type of article:
Original research paper

DOI:
https://doi.org/10.58845/jstt.utt.2026.en.6.2.116-131

***Corresponding author:**
Email address:
vuminhduc@tdtu.edu.vn

Received: 24/09/2025
Received in Revised Form: 15/11/2025
Accepted: 14/12/2025

Abstract: An analytical framework is developed to investigate the nonlinear buckling and postbuckling behavior of sandwich cylindrical panels composed of functionally graded graphene-reinforced composite (FG-GRC) face sheets and a layered corrugated FG-GRC core. The panels are subjected to axial compression and external pressure while resting on Pasternak elastic foundations in a thermal environment. A modified homogenization model is proposed for the layered FG-GRC corrugated core, extending previous formulations of single-layer configurations to include thermal effects. Two types of corrugation geometries, trapezoidal and round, are considered, and various graphene distribution patterns are applied to optimize the stiffness of the FG-GRC core. The governing equations are derived using Donnell-type shell theory in conjunction with von Karman geometric nonlinearity, and the Ritz energy method is employed to obtain the critical buckling load expression and postbuckling equilibrium paths. Parametric studies are conducted to assess the influence of core geometry, graphene distribution, elastic foundation stiffness, thermal effects, and panel dimensions. The results highlight the substantial improvements in structural stability offered by layered corrugated cores and provide valuable insights for the design of advanced FG-GRC sandwich structures under combined mechanical and thermal loads.

Keywords: Functionally graded graphene reinforced composite; Ritz energy method; Donnell shell theory; Buckling and postbuckling; Corrugated core.

1. Introduction

Cylindrical panels reinforced with nanomaterials such as carbon nanotubes (CNTs) or graphene have emerged as promising structural elements due to their exceptional mechanical and thermal properties. By gradually varying the distribution of these reinforcements across the panel thickness, functionally graded nanocomposite structures can be achieved, offering enhanced stiffness, strength, and thermal resistance. Such advanced materials are particularly well-suited for critical applications in

aerospace, marine, and automotive engineering, where components must withstand complex loading environments while maintaining lightweight and reliable performance.

The behavior of functionally graded carbon nanotube-reinforced composite (FG-CNTRC) cylindrical panels resting on Pasternak elastic foundations has been extensively studied using various theoretical approaches. For instance, the higher-order shear deformation theory (HSDT) combined with a two-step perturbation technique was employed to analyze postbuckling responses under axial compression and lateral pressure [1,2], as well as thermal and thermo-mechanical postbuckling scenarios [3,4]. These investigations considered temperature-dependent material properties, five distinct CNT distribution patterns, and geometric nonlinearity based on von Karman assumptions. In addition, the Ritz energy method and first-order shear deformation theory (FSDT) were utilized to examine the free vibration characteristics [5] and dynamic responses under moving loads [6] of FG-CNTRC cylindrical panels, combining with Gram-Schmidt orthogonalization functions. Nonlinear in-plane thermal buckling behavior of FG-CNTRC arches with rotational boundary constraints subjected to uniform radial loads was also investigated using Donnell shell theory [7]. Moreover, three-dimensional elasticity theory, combined with the Fourier series expansions and state-space method, was implemented for thermo-elastic analysis [8] and buckling responses [9], including cases with integrated piezoelectric sensor and actuator layers. Finite element simulations were further conducted to assess the buckling and free vibration behavior under axial, shear [10], and thermal loads [11].

Due to its two-dimensional allotropic structure, graphene exhibits superior interfacial bonding with the surrounding matrix compared to carbon nanotubes, thereby enhancing the overall load transfer efficiency in nanocomposite systems. As a result, functionally graded graphene-reinforced composites (FG-GRC) [12-16] have emerged as promising next-generation candidates within the class of functionally graded materials (FGMs) for advanced structural applications. Extensive research has been conducted on FG-GRC plates using higher-order shear deformation theory (HSDT) in conjunction with perturbation methods to examine bending behavior [12], as well as buckling and postbuckling responses [13]. Building on similar theoretical formulations and solution strategies, nonlinear vibration analyses of FG-GRC cylindrical panels were also reported in [14-16]. Furthermore, the isogeometric finite element method has been employed to study thermal buckling [17], postbuckling behavior [18], and free vibration characteristics [19] of FG-GRC plates. Linear buckling analysis of temperature-dependent FG-GRC laminated plates resting on elastic foundations has also been performed, with attention to the influence of foundation stiffness and thermal environment [20].

Corrugated panel and shell structures constructed from advanced materials have been widely adopted to improve load-carrying capacity while maintaining lightweight characteristics. The trapezoidal and sinusoidal corrugated composite plates were considered by Zheng et al. [21] in problems of supersonic flutter stability, using supersonic piston theory in the framework of Kirchhoff plate theory. Pathirana and Qiao [22,23] investigated the local buckling behavior of sinusoidally corrugated composite panels under different loading conditions, including in-plane shear [22] and uniaxial compression [23], employing the Donnell-type shell theory and Rayleigh-Ritz method. The corrugated structures may also be made from functionally graded materials (FGMs). Notably, corrugated sandwich FGM cylindrical shells were considered in the nonlinear free and forced vibration problems of interacting with internal fluid, using the homogenized corrugation theory developed by Xia et al. [25], and Donnell shell theory, as reported in

[24]. Corrugated cores differ from conventional corrugated configurations in that they act as internal frameworks designed to optimize load distribution and structural efficiency, rather than merely providing surface durability. Such core architectures are especially beneficial in weight-sensitive applications such as aerospace and architectural engineering. Corrugated-core sandwich structures with FG-GRC face sheets have been the focus of several recent studies [26-28]. Employing the Ritz energy method, Donnell shell theory, and the homogenization technique [25], these investigations analyzed the behavior of cylindrical and toroidal sandwich shells subjected to external pressure [26], axial compression or tension [27], and torsional loading [28] in thermal environments. Additionally, the nonlinear buckling responses of FG-CNTRC plates and cylindrical panels with layered corrugated cores have been addressed in [29,30], where the original homogenization approach of Xia et al. [25] was extended to accommodate layered FG-CNTRC configurations.

From the foregoing literature, it is evident that although numerous studies have addressed corrugated structures and sandwich systems incorporating corrugated cores, research on layered corrugated cores remains relatively scarce. This is largely due to the inherent mechanical intricacies and the mathematical complexity involved in modeling such configurations. Notably, the integration of nanocomposite materials, particularly FG-GRC, into corrugated core architectures has received limited attention. Moreover, existing homogenization approaches often fall short in accurately capturing the thermal effects in layered corrugated systems, leaving a significant gap in the current state of the art. Motivated by these challenges, the present study aims to investigate the nonlinear buckling and postbuckling behavior of sandwich cylindrical panels with layered FG-GRC corrugated cores, subjected to external pressure and axial compression, taking into account the thermal stresses. Both trapezoidal and round corrugation geometries are considered for the core layers, with various graphene distributions to optimize structural performance. The governing equations are derived using Donnell-type shell theory in combination with von Karman geometric nonlinearity, while a refined homogenization model is proposed to effectively characterize layered corrugated cores. The Ritz energy method is employed to obtain explicit expressions for critical buckling loads and to trace the postbuckling equilibrium paths. Through comprehensive numerical analyses, the study reveals the significant influence of core geometry, material design, elastic foundation stiffness, and temperature variation on the buckling behavior of FG-GRC sandwich panels. The findings contribute to the design and optimization of advanced lightweight structures for thermomechanical applications.

2. Geometrical and material designs

Considers a panel with two FG-GRC face sheets and three corrugated FG-GRC core layers. The panel is subjected to axial compression P_x and external pressure q in a thermal environment T, placed in the coordinate system as shown in Fig. 1. Two geometrical forms of corrugations, round and trapezoidal, are investigated, and three corrugated core layers are orthogonally arranged.

The thicknesses of the two FG-GRC face sheets are the same, denoted by h_1, and three corrugated core thicknesses are the same, denoted by h_2, the total panel thickness is denoted by h_3, and the corrugation wall thickness is denoted by τ. The half-length of the segment of the round corrugated core, between two arcs, is denoted by δ, and the arc radius is denoted by ι. The half-amplitude of the trapezoidal corrugations is denoted by ψ, and the trough angle of the trapezoidal corrugations is denoted by ϕ. The half-

period and wall thickness of trapezoidal and round corrugations are respectively denoted by ς and τ.

The zigzag direction of graphene/corrugation is in the longitudinal direction of the panel and is defined by (0-layer), while the circumferential direction is defined by (90-layer). The face sheets and corrugated core layers are composed of many GRC layers; only a sample of graphene direction arrangement $(0)_{10}$ is considered, and two corrugation direction arrangements, 0/90/0 and 90/0/90, are investigated. Additionally, three laws of graphene distribution are investigated as UD, FG-X, and FG-O (see Fig. 2). The graphene volume fractions symmetrically varied from the mid-plane of panels, $[0.11/0.09/0.07/0.05/0.03]_S$ defined for the FG-O type and $[0.03/0.05/0.07/0.09/0.11]_S$ defined for the FG-X type. The volume fraction of graphene is constant ($V_G = 0.07$) for all layers for UD graphene distribution type.

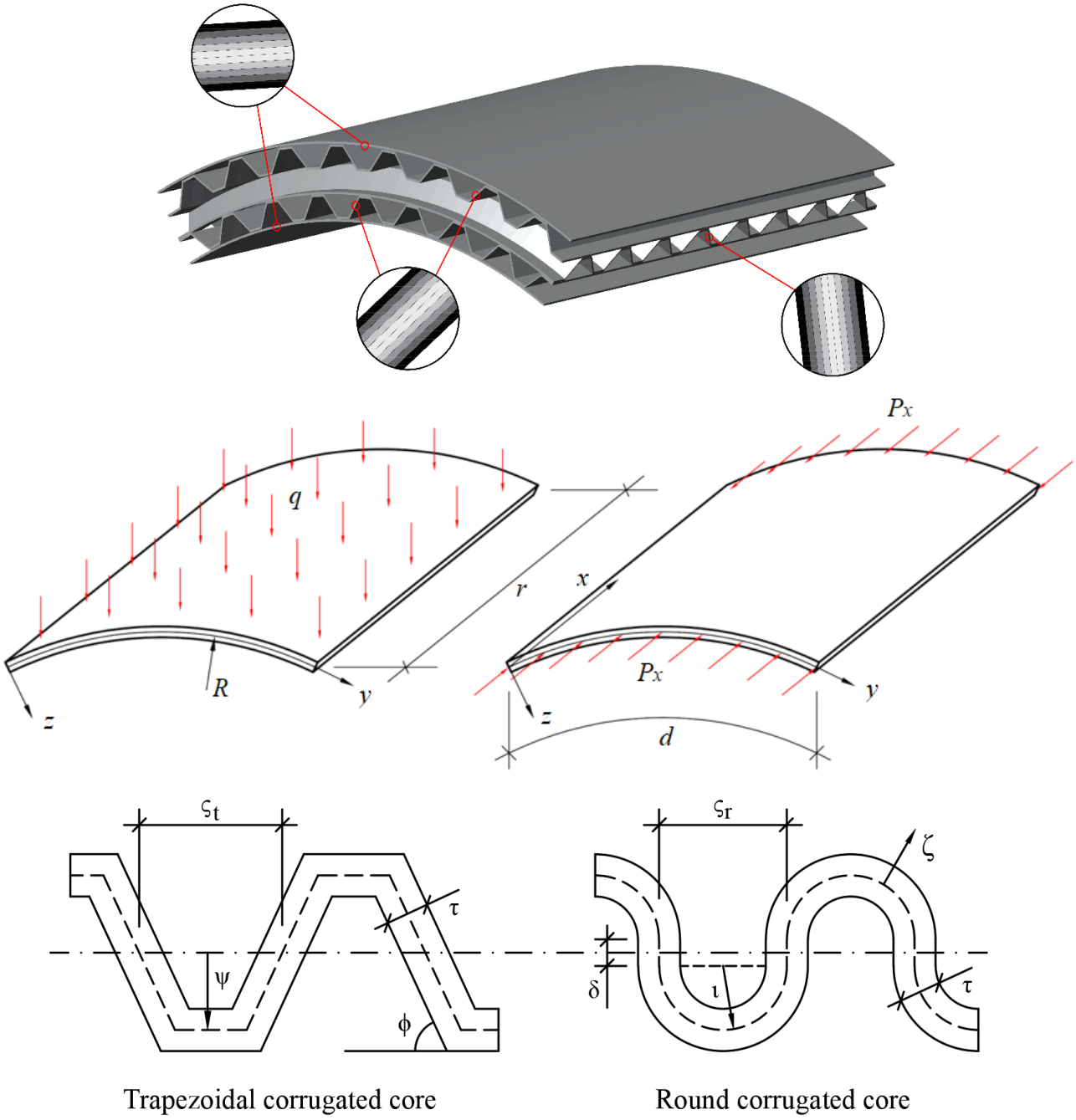

Fig. 1. Geometry and coordinate system of FG-GRC sandwich panels with corrugated FG-GRC core

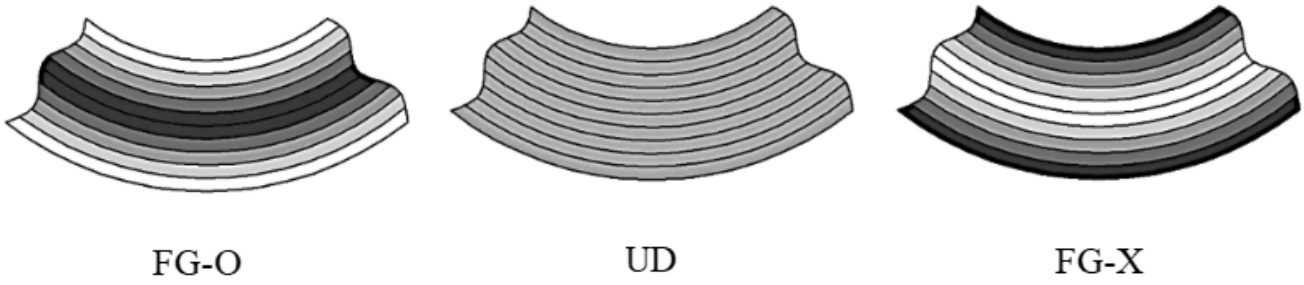

Fig. 2. Graphene distribution laws of face sheets and corrugated cores

By using the expanded Halpin-Tsai model, Young's moduli of FG-GRC layers are estimated, Poisson ratios and thermal expansion coefficients can be predicted by the mixture rule, respectively, as [12-16]

$$E_{11}=\lambda_1 E^{MT}\frac{1+2\gamma_{11}V_{GR}\left(a_{GR}/h_{GR}\right)}{1-V_{GR}\gamma_{11}},$$

$$E_{22}=\lambda_2 E^{MT}\frac{1+2\left(b_{GR}/h_{GR}\right)\gamma_{22}V_{GR}}{1-\gamma_{22}V_{GR}}, \quad (1)$$

$$G_{12}=\frac{\lambda_3 G^{MT}}{1-\gamma_{12}V_{GR}},$$

$$\nu_{12}=\nu_{12}^{GR}V_{GR}+V_{MT}\nu^{MT}, \quad (2)$$

$$\alpha_{11}=\frac{\alpha_{11}^{GR}V_{GR}E_{11}^{GR}+\alpha^{MT}V_{MT}E^{MT}}{V_{GR}E_{11}^{GR}+V_{MT}E^{MT}},$$

$$\alpha_{22}=V_{GR}\alpha_{22}^{GR}\left(1+\nu_{12}^{GR}\right)+V_{MT}\alpha^{MT}\left(1+\nu^{MT}\right) \quad (3)$$

$$-\nu_{12}\alpha_{11},$$

For the orthotropic panels, Hooke's law can be presented by

$$\begin{bmatrix}\sigma_x\\ \sigma_y\\ \sigma_{xy}\end{bmatrix}=\begin{bmatrix}Q_{11} & Q_{12} & 0\\ Q_{12} & Q_{22} & 0\\ 0 & 0 & Q_{66}\end{bmatrix}\left(\begin{bmatrix}\varepsilon_x\\ \varepsilon_y\\ \gamma_{xy}\end{bmatrix}-\begin{bmatrix}\alpha_{11}\\ \alpha_{22}\\ 0\end{bmatrix}\Delta T\right), \quad (4)$$

where Q_{ij} are the reduced stiffnesses, calculated by

$$Q_{11}=\frac{E_{11}}{1-\nu_{21}\nu_{12}},\ Q_{22}=\frac{E_{22}}{1-\nu_{21}\nu_{12}},$$

$$Q_{12}=\frac{\nu_{21}E_{11}}{1-\nu_{21}\nu_{12}},\ Q_{66}=G_{12}.$$

By improving the homogenization technique of Xia et al. [25], the forces and moments of the FG-GRC sandwich panels with corrugated FG-GRC core can be expressed in the orthotropic form using the improved homogenization technique for corrugated cores, taking into account the thermal forces and laminated corrugated layers, presented as

$$\begin{Bmatrix}N_x\\ N_y\\ N_{xy}\\ M_x\\ M_y\\ M_{xy}\end{Bmatrix}=\begin{Bmatrix}H_{11} & H_{12} & 0 & 0 & 0 & 0\\ H_{12} & H_{22} & 0 & 0 & 0 & 0\\ 0 & 0 & H_{66} & 0 & 0 & 0\\ 0 & 0 & 0 & S_{11} & S_{12} & 0\\ 0 & 0 & 0 & S_{12} & S_{22} & 0\\ 0 & 0 & 0 & 0 & 0 & S_{66}\end{Bmatrix}\times \quad (5)$$

$$\begin{Bmatrix}\varepsilon_x^0\\ \varepsilon_y^0\\ \gamma_{xy}^0\\ -\omega_{,xx}\\ -\omega_{,yy}\\ -2\omega_{,xy}\end{Bmatrix}-\begin{Bmatrix}\Theta_{x1}\\ \Theta_{y1}\\ 0\\ 0\\ 0\\ 0\end{Bmatrix},$$

where the stiffnesses of the FG-GRC panels H_{ij}p and S_{ij} can be obtained by totaling the stiffnesses of two FG-GRC face sheets and three corrugated FG-GRC cores, which leads to

$$\left(H_{ij},S_{ij}\right)=\left(H_{ij}^{tf},S_{ij}^{tf}\right)+\left(H_{ij}^{cs[1]},S_{ij}^{cs[1]}\right)$$

$$+\left(H_{ij}^{cs[2]},S_{ij}^{cs[2]}\right)+\left(H_{ij}^{cs[3]},S_{ij}^{cs[3]}\right)+\left(H_{ij}^{bf},H_{ij}^{bf}\right),$$

$$\left(\Theta_{x1},\Theta_{y1}\right)=\left(\Theta_{x1}^{tf},\Theta_{y1}^{tf}\right)+\left(\Theta_{x1}^{cs[1]},\Theta_{y1}^{cs[1]}\right) \quad (6)$$

$$+\left(\Theta_{x1}^{cs[2]},\Theta_{y1}^{cs[2]}\right)+\left(\Theta_{x1}^{cs[3]},\Theta_{y1}^{cs[3]}\right)+\left(\Theta_{x1}^{bf},\Theta_{y1}^{bf}\right),$$

for the face sheets

$$\left(H_{ij}^{tf},S_{ij}^{tf}\right)=\int_{-\frac{h_3}{2}}^{-\frac{h_2}{2}}Q_{ij}^{tf}\left(1,z^2\right)dz,$$

$$\left(H_{ij}^{bf}, S_{ij}^{bf}\right) = \int_{\frac{h_2}{2}}^{\frac{h_3}{2}} Q_{ij}^{bf}\left(1, z^2\right) dz, \quad (i,j) = (1,2,6),$$

$$\Theta_{1x}^{tf} = \int_{-\frac{h_3}{2}}^{-\frac{h_2}{2}} \left(Q_{11}^{tf}\alpha_{11}^{tf} + Q_{12}^{tf}\alpha_{22}^{tf}\right) dz,$$

$$\Theta_{1x}^{lo} = \int_{\frac{h_2}{2}}^{\frac{h_3}{2}} \left(Q_{11}^{bf}\alpha_{11}^{bf} + Q_{12}^{bf}\alpha_{22}^{bf}\right) dz,$$

$$\Theta_{1y}^{tf} = \int_{-\frac{h_3}{2}}^{-\frac{h_{cs}}{2}} \left(Q_{12}^{tf}\alpha_{11}^{tf} + Q_{22}^{tf}\alpha_{22}^{tf}\right) dz,$$

$$\Theta_{1y}^{bf} = \int_{\frac{h_{cs}}{2}}^{\frac{h_3}{2}} \left(Q_{12}^{bf}\alpha_{11}^{bf} + Q_{22}^{bf}\alpha_{22}^{bf}\right) dz,$$

and the stiffness components $H_{ij}^{cs[1]}, H_{ij}^{cs[2]}, H_{ij}^{cs[3]}$, $S_{ij}^{cs[1]}, S_{ij}^{cs[2]}, S_{ij}^{cs[3]}$ and the thermal forces $\Theta_{x1}^{cs[1]}, \Theta_{x1}^{cs[2]}, \Theta_{x1}^{cs[3]}, \Theta_{y1}^{cs[1]}, \Theta_{y1}^{cs[2]}, \Theta_{y1}^{cs[3]}$ with $k = (1,2,3)$ is the order of the cores, with

- for x-directional cores

$$H_{22}^{cs[k]} = \frac{2\varsigma}{l_1/H_{11} + l_2/\bar{S}_{11}}, \; H_{12}^{cs[k]} = \frac{H_{22}^{cs[k]}\bar{H}_{12}}{\bar{H}_{11}},$$

$$H_{11}^{cs[k]} = \frac{l}{\varsigma}\frac{\bar{H}_{11}\bar{H}_{22} - \bar{H}_{12}^2}{\bar{H}_{11}} + \frac{H_{12}^{cs[k]}\bar{H}_{12}}{\bar{H}_{11}},$$

$$H_{66}^{cs[k]} = \frac{\varsigma}{l}\bar{H}_{66}, \quad S_{22}^{cs[2]} = \frac{\varsigma}{l}\bar{S}_{11},$$

$$S_{12}^{cs[2]} = \frac{\bar{S}_{12}}{\bar{S}_{11}} S_{22}^{cs[2]}, \; S_{11}^{cs[2]} = \frac{1}{2\varsigma}\left(l_2\bar{H}_{22} + l_1\bar{S}_{22}\right),$$

$$S_{66}^{cs[2]} = \frac{l}{\varsigma}\bar{S}_{66}, \; S_{ij}^{cs[1]} = \int_{-\frac{h_2}{2}}^{-\frac{h_2}{6}} Q_{ij}^{*cs} z^2 dz,$$

$$S_{ij}^{cs[3]} = \int_{\frac{h_2}{6}}^{\frac{h_2}{2}} Q_{ij}^{*cs} z^2 dz,$$

$$\Theta_{x1}^{cs[k]} = H_{11}^{cs[k]}\bar{\alpha}_{11}^{cs} + H_{12}^{cs[k]}\bar{\alpha}_{22}^{cs},$$

$$\Theta_{y1}^{cs[k]} = H_{12}^{cs[k]}\bar{\alpha}_{11}^{cs} + H_{22}^{cs[k]}\bar{\alpha}_{22}^{cs}, \tag{7}$$

- for y-directional cores

$$H_{11}^{cs[k]} = \frac{2\varsigma}{l_1/H_{11} + l_2/\bar{S}_{11}}, \; H_{12}^{cs[k]} = \frac{H_{11}^{cs[k]}\bar{H}_{12}}{\bar{H}_{11}},$$

$$H_{22}^{cs[k]} = \frac{l}{\varsigma}\frac{\bar{H}_{11}\bar{H}_{22} - \bar{H}_{12}^2}{\bar{H}_{11}} + \frac{H_{12}^{cs[k]}\bar{H}_{12}}{\bar{H}_{11}},$$

$$H_{66}^{cs[k]} = \frac{\varsigma}{l}\bar{H}_{66}, \; S_{11}^{cs[2]} = \frac{\varsigma}{l}\bar{S}_{11}, \; S_{12}^{cs[2]} = \frac{\bar{S}_{12}}{\bar{S}_{11}} S_{11}^{cs[2]},$$

$$S_{22}^{cs[2]} = \frac{1}{2\varsigma}\left(l_2\bar{H}_{22} + l_1\bar{S}_{22}\right),$$

$$S_{66}^{cs[2]} = \frac{l}{\varsigma}\bar{S}_{66}, \; S_{ij}^{cs[1]} = \int_{-\frac{h_2}{2}}^{-\frac{h_2}{6}} Q_{ij}^{*cs} z^2 dz,$$

$$S_{ij}^{cs[3]} = \int_{\frac{h_2}{6}}^{\frac{h_2}{2}} Q_{ij}^{*cs} z^2 dz,$$

$$\Theta_{y1}^{cs[k]} = H_{11}^{cs[k]}\bar{\alpha}_{11}^{cs} + H_{12}^{cs[k]}\bar{\alpha}_{22}^{cs},$$

$$\Theta_{x1}^{cs[k]} = H_{12}^{cs[k]}\bar{\alpha}_{11}^{cs} + H_{22}^{cs[k]}\bar{\alpha}_{22}^{cs}, \tag{8}$$

in which

- for trapezoidal corrugation

$$\varsigma = \varsigma_t, \; l = \varsigma + 2\psi\left(\frac{1}{\sin\phi} - \frac{1}{\tan\phi}\right),$$

$$l_1 = -\frac{8\psi\cos\phi}{3\sin\phi} + 2\varsigma, \; l_2 = 2\psi^2\left(\varsigma - \frac{2\psi}{\tan\phi}\right) + \frac{4\psi^3}{3\sin\phi},$$

- for round corrugation

$$\varsigma = \varsigma_r = 2l, \; l = \pi l + 2\delta, \; l_1 = \pi l,$$
$$l_2 = \pi l^3 + 8\delta l^2 + 2\pi\delta^2 l + 4\delta^3/3.$$

and

$$\left(\bar{H}_{ij}, \bar{S}_{ij}\right) = \int_{-\frac{\tau}{2}}^{\frac{\tau}{2}} Q_{ij}^{cs}\left(1, \zeta^2\right) d\zeta, \quad \left(\bar{\alpha}_{11}^{cs}, \bar{\alpha}_{22}^{cs}\right)$$
$$= \frac{1}{\tau}\int_{-\frac{\tau}{2}}^{\frac{\tau}{2}} \left(\alpha_{11}, \alpha_{22}\right) d\zeta, \; Q_{ij}^{*cs} = \frac{12}{\left(h_2/3\right)^3} S_{ij}^{cs[2]}, \tag{9}$$

Note that: in Eq. (9), for y-directional cores, the stiffnesses $S_{ij}^{cs[2]}$ are determined from Eq. (7), and those are calculated from Eq. (8) for x-directional corrugated cores.

3. Theoretical fundamentals

The compatibility equation of the panels,

according to Donnell shell theory, is obtained by

$$\varepsilon^0_{x,yy}+\varepsilon^0_{y,xx}-\gamma^0_{xy,xy}=\omega^2_{,xy}-\frac{\omega_{,xx}}{R}-\omega_{,xx}\omega_{,yy} -\omega_{,xx}\omega^*_{,yy}+2\omega_{,xy}\omega^*_{,xy}-\omega^*_{,xx}\omega_{,yy}. \quad (10)$$

The introduced stress function $\varphi(x,y)$ satisfies the following conditions

$$N_x=\varphi_{,yy},\ N_y=\varphi_{,xx},\ N_{xy}=-\varphi_{,xy}. \quad (11)$$

The four simply supported and freely movable edges are considered in this paper, with the boundary conditions applied as

$$\begin{aligned} &N_x=N_{x0}=-h_3P_x, M_x\big|_{x=0,r}=0, N_{xy}\big|_{x=0,r}=0,\\ &\omega\big|_{x=0,r}=0, N_y=N_{y0}=0, M_y\big|_{y=0,d}=0,\\ &N_{xy}\big|_{y=0,d}=0, \omega\big|_{y=0,d}=0. \end{aligned} \quad (12)$$

A trigonometric function is adopted to represent the deflection pattern, and the initial imperfection is assumed to share the same functional form, given by

$$\begin{aligned} &\omega=W\sin\alpha x\sin\beta y,\\ &\omega^*=\xi h_3\sin\alpha x\sin\beta y, \end{aligned} \quad (13)$$

where m and n are the buckling modes, $\alpha=\frac{\pi}{r}m,\ \beta=\frac{\pi}{d}n$.

The compatibility equation (10) is rewritten as

$$H^*_{22}\varphi_{,xxxx}+\left(2H^*_{12}+H^*_{66}\right)\varphi_{,xxyy}+H^*_{11}\varphi_{,yyyy}+\frac{\omega_{,xx}}{R} -\omega^2_{,xy}+\omega_{,xx}\omega_{,yy}+\omega_{,xx}\omega^*_{,yy}-2\omega_{,xy}\omega^*_{,xy}+\omega^*_{,xx}\omega_{,yy}=0. \quad (14)$$

where

$$H^*_{11}=\frac{H_{22}}{H_{11}H_{22}-H^2_{12}},\ H^*_{12}=\frac{-H_{12}}{H_{11}H_{22}-H^2_{12}},$$
$$H^*_{22}=\frac{H_{11}}{H_{11}H_{22}-H^2_{12}},\ H^*_{66}=\frac{1}{H_{66}},$$

Substituting the solution forms (13) into Eq. (14) and applying the harmonic balance method, the stress function φ is obtained as

$$\varphi=\varphi_1\cos\frac{2m\pi x}{r}+\varphi_2\cos\frac{2n\pi y}{d} +\varphi_3\sin\frac{m\pi x}{r}\sin\frac{n\pi y}{d}+\frac{N_{x0}y^2}{2}. \quad (15)$$

where

$$\varphi_1=\frac{1}{16}\frac{n\pi^2r^2h_3\xi}{d^2m\pi^2H^*_{22}}W+\frac{1}{32}\frac{n\pi^2r^2}{d^2m\pi^2h^*_{22}}W^2,$$

$$\varphi_2=\frac{1}{32}\frac{m\pi^2d^2}{r^2m\pi^2H^*_{22}}W^2+\frac{1}{16}\frac{m\pi^2d^2h_3\xi}{r^2n\pi^2H^*_{22}}W,$$

$$\varphi_3=d^4r^2m\pi^2W\Big/\Big[m\pi^4H^*_{22}d^4R+n\pi^4H^*_{11}r^4R +d^2r^2n\pi^2\left(H^*_{66}+H^*_{12}+H^*_{21}\right)m\pi^2R\Big]$$

The strain energy and the work done by external loads of the FG-GRC panels are expressed, respectively, by

$$U_{int}=\frac{1}{2}\int_{-\frac{h_3}{2}}^{\frac{h_3}{2}}\int_0^d\int_0^r\Big[\sigma_x\left(\varepsilon_x-\alpha_{11}\Delta T\right) +\sigma_y\left(\varepsilon_y-\alpha_{22}\Delta T\right)+\sigma_{xy}\gamma_{xy}\Big]dxdydz, \quad (16)$$

$$U_{ext}=\int_0^d\int_0^r q\omega dxdy+N_{x0}\int_0^d\int_0^r u_{,x}dxdy -\int_0^d\int_0^r\left[\frac{1}{2}\left(C_1\omega^2-C_2\left(\omega_{,xx}+\omega_{,yy}\right)\omega\right)\right]dxdy, \quad (17)$$

where the Winkler and Pasternak foundation parameters are denoted by C_1, C_2, respectively.

The total potential energy can be obtained as

$$U=U_{int}-U_{ext}. \quad (18)$$

Applying the Ritz energy method to the total potential energy, as

$$\frac{\partial U}{\partial W}=0, \quad (19)$$

leads to

$$\Gamma_{11}W+\Gamma_{12}W\left(W+\frac{4}{3}\xi h_3\right) +\Gamma_{13}W\left(2h_3\xi+W\right)\left(h_3\xi+W\right) +\Gamma_{14}q-\Gamma_{15}P_xh_3\left(h_3\xi+W\right)=0, \quad (20)$$

where

$$\Gamma_{11}=\frac{rd}{4}\left\{\begin{aligned} &\left[{O_{31}}^2\left(2H^*_{12}+H^*_{66}\right)+2S_{12}+4S_{66}\right]\beta^2\alpha^2\\ &+\left(H^*_{11}{O_{31}}^2+S_{22}\right)\beta^4+\left(\alpha^2+\beta^2\right)C_2\\ &+C_1+\left(H^*_{22}{O_{31}}^2+S_{11}\right)\alpha^4 \end{aligned}\right\},$$

$$\Gamma_{12} = -\frac{4\chi_n\chi_m O_{31}}{\alpha\beta}\begin{bmatrix} O_{11}H_{22}^*\alpha^4 + O_{21}H_{11}^*\beta^4 \\ +H_{12}^*\left(O_{11}+O_{21}\right)\alpha^2\beta^2 \end{bmatrix},$$

$$\Gamma_{13} = 16rd\left(O_{11}{}^2\alpha^4 H_{22}^* + O_{21}{}^2\beta^4 H_{11}^*\right),$$

$$\Gamma_{14} = \frac{9rd}{64}, \quad \Gamma_{15} = -\frac{\chi_m\chi_n}{\alpha\beta},$$

$$\chi_m = (-1)^m - 1, \ \chi_n = (-1)^n - 1,$$

$$O_{11} = \frac{1}{32}\frac{n\pi^2 r^2}{d^2 m\pi^2 H_{22}^*}, \ O_{21} = \frac{1}{32}\frac{m\pi^2 d^2}{r^2 n\pi^2 H_{11}^*},$$

$$O_{31} = d^4 r^2 m\pi^2 \Big/ \Big[m\pi^4 H_{22}^* d^4 R + n\pi^4 H_{11}^* r^4 R + d^2 r^2 n\pi^2\left(H_{66}^* + H_{12}^* + H_{21}^*\right)m\pi^2 R\Big].$$

The compressive postbuckling expression is determined by using Eq. (28), as

$$P_x = \frac{\Gamma_{11}W + \Gamma_{12}W\left(W + 4h_3\xi/3\right)}{\Gamma_{15}h_3\left(h_3\xi + W\right)} + \frac{\Gamma_{13}W\left(2h_3\xi + W\right)\left(h_3\xi + W\right) + \Gamma_{14}q}{\Gamma_{15}h_3\left(h_3\xi + W\right)}. \quad (21)$$

For perfect panels $(\xi = 0)$, according to the bifurcation buckling phenomenon, the compressive buckling load is determined by applying $W \to 0$, as

$$P_x^{upp} = \Gamma_{11}/\left(\Gamma_{15}h_3\right). \quad (22)$$

Similarly, from Eq. (20), the external pressure postbuckling expression is obtained by

$$q = \frac{\Gamma_{15}P_x h_3\left(h_3\xi + W\right)}{\Gamma_{14}} - \frac{\Gamma_{12}W\left(W + \frac{4}{3}\xi h_3\right)}{\Gamma_{14}} - \frac{\Gamma_{11}W + \Gamma_{13}W\left(2\xi h_3 + W\right)\left(\xi h_3 + W\right)}{\Gamma_{14}}. \quad (23)$$

The minimum compressive buckling loads $P_x^{upp}(m,n)$ from Eq. (22), are defined by the critical buckling load P_x^{ct}.

4. Numerical examples

Table 1 presents a comparison of the critical buckling loads for unstiffened SUS304 cylindrical panels under various geometric conditions. The numerical results obtained from the present analytical approach are validated against previously published data by Shen et al. [31] and Thang et al. [32], where the same boundary conditions and material properties are adopted. These comparisons confirm that the present approach can accurately capture the global buckling behavior of cylindrical panels under thermal and mechanical loading conditions.

Table 2 presents a comparison of the critical buckling loads between FG-GRC cylindrical panels with layered corrugated cores and their equivalent non-corrugated counterparts. Two corrugation geometries, trapezoidal and round, are investigated, along with two core stacking sequences (0/90/0 and 90/0/90) and three graphene distribution types (FG-O, UD, FG-X). For the 0/90/0 configuration, incorporating a trapezoidal corrugated core significantly improves the buckling performance. For example, in the FG-O case, the critical load increases from 64.850 MPa to 77.547 MPa, corresponding to a 19.6% enhancement. The UD and FG-X distributions further increase the loads to 82.184 MPa and 77.815 MPa, yielding relative improvements of 20.2% and 17.9%, respectively. This demonstrates the stiffening effect of the corrugated architecture, which enhances flexural rigidity by increasing the effective distance between the face sheets. A similar trend is observed for round corrugation cores, although the improvement is slightly less pronounced due to their smoother curvature and smaller structural depth. In the 0/90/0 stacking scheme, the FG-O type increases from 70.001 MPa to 79.280 MPa (13.3%), while the UD and FG-X types reach 84.081 MPa and 79.561 MPa, with improvements of 13.6% and 12.4%, respectively. For the 90/0/90 core arrangement, where the outer layers are oriented circumferentially, the critical loads are lower than in the 0/90/0 case. Nonetheless, the corrugated cores still outperform their non-corrugated counterparts. For instance, the trapezoidal FG-O panel increases from 64.816 MPa to 72.695 MPa (12.2%), and the round FG-O

panel increases from 69.918 MPa to 72.934 MPa (4.3%). These results indicate that the layered corrugated architecture enhances the buckling resistance across all configurations, albeit to varying degrees depending on the geometric and material parameters.

Table 1. Comparisons of critical buckling loads $\bar{P}_x^{cr} = P_x^{cr} bh$ (MN) of unstiffened SUS304 cylindrical panels ($b = 0.3$m, $\Delta T = 0$K).

a/R_c	b/h	References	
0.5	30	Shen et al. [31]	4.9565 (1,1)*
		Thang et al. [32]	5.207
		Present	5.232 (1,1)
1.0	30	Shen et al. [31]	10.2899 (3,1)
		Thang et al. [32]	10.414
		Present	10.374 (3,1)
0.5	0.6	Shen et al. [31]	1.2968 (1,3)
		Thang et al. [32]	1.301
		Present	1.308 (3,1)

* Buckling mode (m,n)

Table 2. Comparisons of critical buckling loads P_0^{cr} of layered corrugated core and of the equivalent non-corrugated core (MPa, $r = d = 100h_3$, $T = 400$K, $m = n = 1$, $h_3 = 21$mm, $R = 10r$, $h_2 = 15$mm, h_1=3mm, $\tau = 1$mm, $\psi = 2$mm, $\varsigma_t = 4\psi$, $\phi = \pi/4$, $\iota = 1.4$mm, $\delta = 0.6$mm, $\varsigma_r = 2\iota$, $C_1 = 10$ MN/m^3, $C_2 = 0.1$ MN/m)

	Trapezoidal corrugation			Round corrugation		
	FG-O	UD	FG-X	FG-O	UD	FG-X
	Corrugated cores					
0/90/0	77.547[a](19.6)**	82.184[a](20.2)	77.815[a](17.9)	79.280[a](13.3)	84.081[a](13.6)	79.561[a](12.4)
90/0/90	72.695[a](12.2)	76.848[a](12.4)	72.971[a](10.6)	72.934[a](4.3)	77.077[a](4.2)	73.191[a](3.5)
	Equivalent non-corrugated cores					
0/90/0	64.850[b]	68.357[b]	65.987[b]	70.001[c]	74.025[c]	70.800[c]
90/0/90	64.816[b]	68.350[b]	65.952[b]	69.918[c]	73.988[c]	70.714[c]

** The difference (%) between critical buckling loads of the corrugated core and of the equivalent non-corrugated core; [a] The buckling mode (3,1); [b] The buckling mode (5,1); [c] The buckling mode (4,1)

Table 3 investigates the influence of thermal environment on the critical buckling loads of FG-GRC cylindrical panels with layered corrugated cores, considering both trapezoidal and round corrugation types under the 0/90/0 graphene orientation configuration. Three graphene distribution laws, including FG-O, UD, and FG-X, are examined at environmental temperatures of 300 K, 400 K, and 500 K. As expected, increasing temperature results in a notable reduction in the critical buckling loads across all configurations. This trend is primarily attributed to the thermal softening effect, where the effective stiffness of both the graphene-reinforced composite and the entire structure decreases due to elevated temperatures. For instance, in the trapezoidal FG-

O panel, the critical load drops from 83.413 MPa at 300 K to 76.068 MPa at 500 K, indicating an approximate 8.8% reduction. Similar reductions are observed in the UD and FG-X distributions, highlighting the thermal sensitivity of the structure regardless of the graphene gradation pattern. Comparatively, round corrugation cores show slightly higher critical loads at each temperature level than their trapezoidal counterparts. For example, at 300 K, the round UD panel achieves 90.918 MPa, compared to 88.787 MPa in the trapezoidal case. This trend persists at elevated temperatures, although the differences remain marginal. The smoother curvature of round corrugation likely provides a more uniform stress distribution, contributing to its marginally superior performance under thermal loads. Among the distribution laws, UD panels exhibit the highest critical buckling loads, followed closely by FG-X, while FG-O consistently results in the lowest values at all temperatures. This observation aligns with the fact that UD distributions maintain a constant graphene volume fraction throughout the thickness, thereby ensuring maximum stiffness near the outermost layers, which are critical under bending-dominated buckling.

Table 3. Effects of thermal environment on the critical buckling loads P_0^{cr} (MPa, (0/90/0) panels, $r = d = 100h_3$, $m = 3, n = 1$, $h_3 = 21mm$, $R = 10r$, $h_2 = 15mm$, h_1=3mm, $\tau = 1mm$, $\psi = 2mm$, $\varsigma_t = 4\psi$, $\phi = \pi/4$, $\iota = 1.4mm$, $\delta = 0.6mm$, $\varsigma_r = 2\iota$, $C_1 = 10$ MN/m^3, $C_2 = 0.1$ MN/m)

	Trapezoidal corrugation			Round corrugation		
T (K)	FG-O	UD	FG-X	FG-O	UD	FG-X
300	83.413	88.787	83.717	85.347	90.918	85.668
400	77.547	82.184	77.815	79.280	84.081	79.561
500	76.068	80.162	76.325	77.753	81.997	78.021

Table 4 explores the effect of geometrical parameters of the layered corrugated core, specifically the corrugation amplitude and core thickness, on the critical buckling loads of FG-GRC cylindrical panels. Both trapezoidal and round corrugation configurations are analyzed under the 90/0/90 orientation of graphene layers, with all three graphene distribution laws (FG-O, UD, FG-X) considered. For trapezoidal corrugations, an increase in both the half-amplitude ψ and the core thickness h_2 (from 2 mm/15 mm to 3 mm/21 mm) leads to a progressive and substantial rise in the critical buckling loads. For instance, in the FG-O case, the critical load improves from 72.695 MPa to 80.554 MPa, which corresponds to an increase of approximately 10.8%. Similar trends are observed in the UD and FG-X cases. This enhancement is due to the increased moment of inertia and structural depth offered by the higher core and corrugation geometry, which improves the overall bending rigidity of the panel. In the case of round corrugations, a similar pattern emerges with respect to the parameters δ and h_2, representing the transition arc length and core height, respectively. The critical load in the FG-O configuration increases from 69.903 MPa (at δ=0 mm, h_2=11.4 mm) to 80.946 MPa (at =1.6 mm, h_2=21 mm), indicating a 15.8% improvement. Notably, the round cores respond more sensitively to changes in geometry compared to trapezoidal cores, likely due to their initially lower stiffness at smaller geometric scales. Across both geometries, the FG-X panels consistently demonstrate the highest critical buckling loads, followed by UD and FG-O types. This observation aligns with earlier results and reinforces the importance of placing higher graphene volume fractions near the face layers, as in the FG-X distribution, to optimize bending stiffness.

Table 4. Effects of geometrical parameters of corrugated core on the critical buckling loads P_0^{cr} (MPa, (90/0/90) panels, $r = d = 100h_3$, $m = 3, n = 1$, $R = 10r$, h_1=3mm, $\tau = 1$mm, $\varsigma_t = 4\psi$, $\phi = \pi/4$, $\iota = 1.4$mm, $\varsigma_r = 2\iota$, $C_1 = 10$ MN/m^3, $C_2 = 0.1$ MN/m)

	FG-O	UD	FG-X
Trapezoidal corrugation			
ψ = 2mm, h_2 = 15mm	72.695	76.848	72.971
ψ = 2.5mm, h_2 = 18mm	76.658	81.489	76.898
ψ = 3mm, h_2 = 21mm	80.554	83.560	80.674
Round corrugation			
δ = 0 mm, h_2 = 11.4mm	69.903	73.259	70.224
δ = 0.6mm, h_2 = 15mm	72.934	77.077	73.191
δ = 1.6 mm, h_2 = 21mm	80.946	83.945	81.063

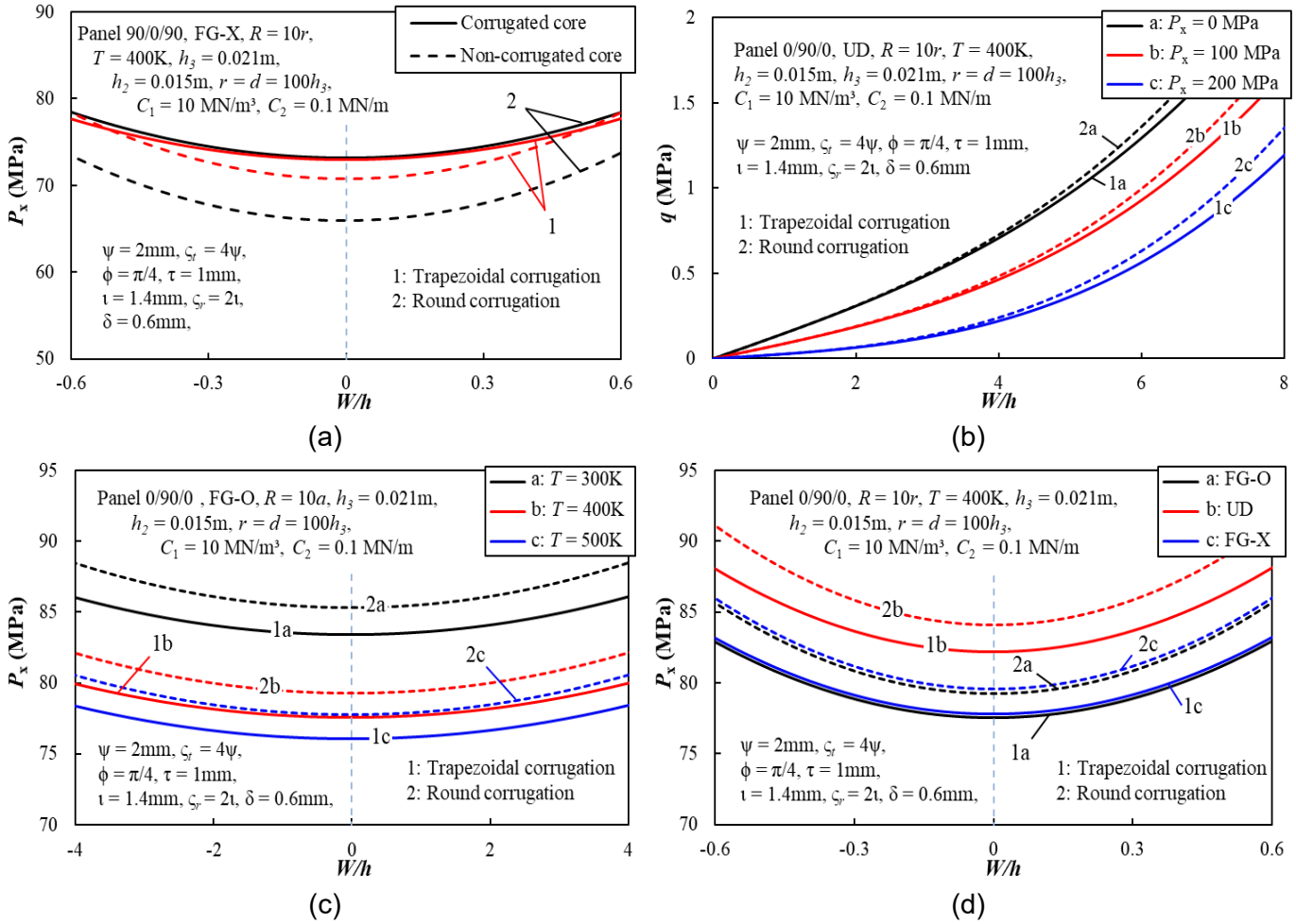

Fig. 3. Effects of corrugated core and corrugation types on the postbuckling responses of panels

Fig. 3 presents a comprehensive analysis of the compression and pressure postbuckling behaviors of FG-GRC sandwich cylindrical panels with layered corrugated cores. Fig. 3(a) compares the postbuckling responses between panels with layered corrugated cores and their equivalent non-corrugated counterparts under axial compression. The corrugated core panels clearly exhibit superior

postbuckling strength, particularly in the large-deflection regime. This improvement is attributed to the enhanced bending stiffness introduced by the corrugated structure, which increases the effective distance between the face sheets and offers better resistance against geometric nonlinearity. The comparison validates the effectiveness of adopting corrugated core designs in improving both stability and load-carrying capacity. Fig. 3(b) investigates the influence of pre-compressive axial loads on the postbuckling behavior under subsequent external pressure. It is observed that increasing the pre-compression level leads to a noticeable reduction in postbuckling strength. This is due to the accumulation of compressive stresses, which lowers the panel's residual capacity to withstand additional pressure loading. Fig. 3(c) analyzes the impact of thermal environment on the compression postbuckling response. As the ambient temperature increases, the postbuckling strength decreases considerably, especially in the nonlinear deformation zone. This trend is a consequence of temperature-induced material softening, where both the graphene reinforcement and matrix experience a reduction in stiffness. Fig. 3(d) examines the effect of different graphene volume fraction distribution laws, namely UD, FG-X, and FG-O, on the postbuckling response under axial compression. The FG-X distribution results in the highest postbuckling strength, followed by UD and then FG-O. This outcome aligns with the expectation that concentrating more graphene near the face sheets, as in FG-X, enhances flexural rigidity, which is critical for postbuckling resistance. Meanwhile, the symmetric FG-O distribution shows the weakest performance due to the relatively lower stiffness near the surfaces, which are the most stressed regions during bending.

Fig. 4 illustrates the effects of geometrical parameters of the panel, specifically the axial length and circumferential length, on the postbuckling responses of FG-GRC sandwich cylindrical panels under both axial compression and external pressure. The results are presented for representative cases to evaluate how changes in overall panel dimensions influence postbuckling strength and stability. Fig. 4(a) demonstrates the impact of increasing the axial length on the panel's postbuckling response under axial compression. As axial length increases, the postbuckling strength gradually decreases, especially in the large-deflection range. This behavior is attributed to the reduction in global stiffness as the structure becomes more slender, making it more susceptible to global buckling modes and geometric nonlinearity. Fig. 4(b) presents the same trend under external pressure loading. As the axial length increases, the panel exhibits lower postbuckling resistance, indicating that slender panels offer less support against transverse loads, particularly after initial buckling. The longer the panel, the more pronounced the deflection and energy absorption, which reduces the effective stiffness in the postbuckling regime.

Fig. 5 presents the effects of elastic foundation parameters on the postbuckling responses of FG-GRC sandwich cylindrical panels with layered corrugated cores, considering two distinct scenarios: axial compression with trapezoidal cores (Fig. 5a) and external pressure with round cores (Fig. 5b). In both cases, the role of the elastic foundation stiffness, specifically the Winkler modulus and Pasternak shear layer modulus, is investigated. In Fig. 5(a), under axial compression, increasing the stiffness of the Winkler and Pasternak foundation results in a clear enhancement of postbuckling strength for the panels with trapezoidal cores. The stiffer foundation provides greater resistance against transverse deformation, thereby limiting the amplitude of postbuckling deflections and increasing the effective stiffness in the nonlinear regime. In Fig. 5(b), a similar stabilizing trend is observed under external pressure loading for

panels with round corrugated cores. As the foundation parameters increase, the panel becomes more resistant to outward deformation and maintains structural integrity beyond the initial buckling point. Compared to the compression case, the pressure-loaded panels show more sensitivity to foundation stiffness, indicating that elastic support is especially crucial in pressure-dominated scenarios, where transverse deflection plays a dominant role in structural response.

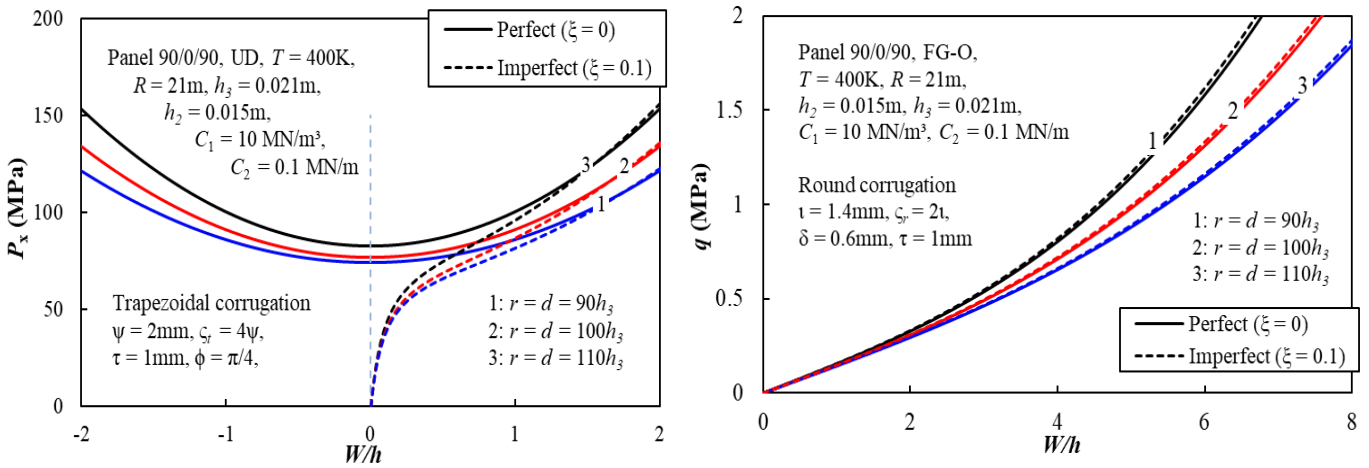

Fig. 4. Effects of geometrical parameters of panels on the postbuckling responses

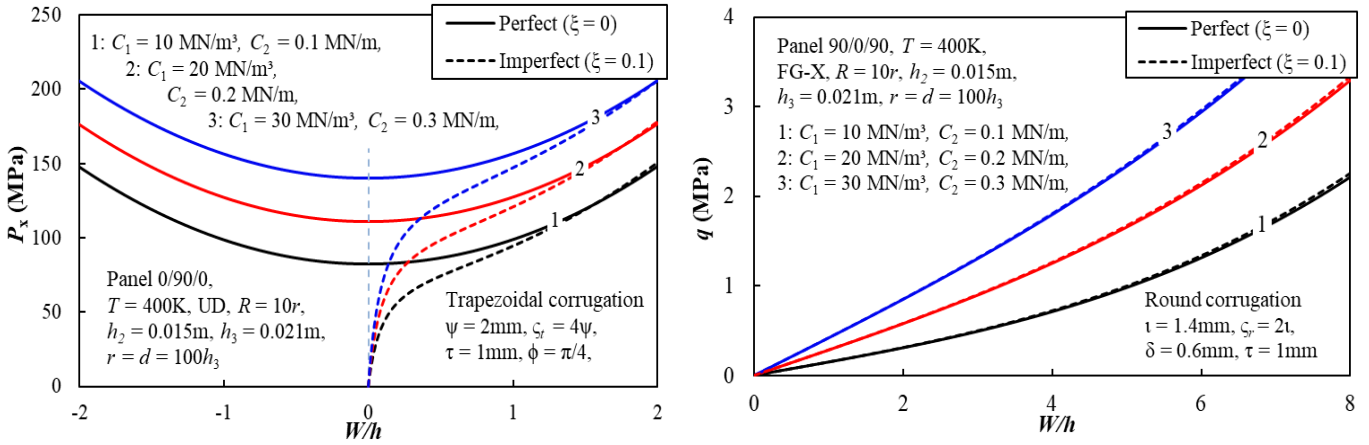

Fig. 5. Effects of elastic foundation parameters of corrugations on the postbuckling responses of panels

5. Conclusion

This study presents an analytical investigation into the nonlinear buckling and postbuckling behaviors of sandwich cylindrical panels with layered corrugated FG-GRC cores, subjected to axial compression and external pressure in a thermal environment. A homogenization model originally developed for single-layer corrugated cores is extended and improved to account for layered configurations and various graphene distribution laws. The governing equations are derived based on Donnell shell theory incorporating von Karman geometric nonlinearity, and solved using the Ritz energy method. Key conclusions drawn from the numerical analyses are as follows:

Layered corrugated cores significantly enhance both critical buckling loads and postbuckling strength compared to equivalent non-corrugated cores. This improvement is more pronounced for trapezoidal cores due to their larger structural depth and bending stiffness.

The graphene distribution law plays a crucial role in mechanical performance. The FG-X pattern, which concentrates graphene near the outer layers, consistently provides superior buckling and postbuckling resistance compared to FG-O and UD configurations.

Increasing the ambient temperature leads to a substantial reduction in buckling capacity due to material softening. Nevertheless, round corrugated cores demonstrate slightly better thermal stability than trapezoidal ones.

Enhanced core geometry, such as increasing corrugation amplitude or core thickness, leads to notable gains in buckling performance. Round cores are particularly sensitive to geometric refinement, offering high efficiency when optimized.

The global dimensions of the panel, especially the axial length, markedly affect postbuckling behavior. Longer panels exhibit reduced postbuckling strength under both compressive and pressure loads due to lower global stiffness.

Elastic foundations, modeled via Winkler and Pasternak parameters, effectively increase postbuckling resistance. This stabilizing effect is more critical in panels subjected to external pressure and can be tailored to improve structural safety.

References

[1] H.S. Shen, Y. Xiang. (2014). Postbuckling of axially compressed nanotube-reinforced composite cylindrical panels resting on elastic foundations in thermal environments. *Composites Part B: Engineering*, 67, 50-61. https://doi.org/10.1016/j.compositesb.2014.06.020

[2] H.S. Shen. (2016). Postbuckling of nanotube-reinforced composite cylindrical panels resting on elastic foundations subjected to lateral pressure in thermal environments. *Engineering Structures*, 122, 174-183. https://doi.org/10.1016/j.engstruct.2016.05.004

[3] H.S. Shen, Y. Xiang. (2015). Thermal postbuckling of nanotube-reinforced composite cylindrical panels resting on elastic foundations. *Composite Structures*, 123, 383-392. https://doi.org/10.1016/j.compstruct.2014.12.059

[4] H. Babaei. (2022). Thermomechanical analysis of snap-buckling phenomenon in long FG-CNTRC cylindrical panels resting on nonlinear elastic foundation. *Composite Structures*, 286, 115199. https://doi.org/10.1016/j.compstruct.2022.115199

[5] M. Mirzaei, Y. Kiani. (2016). Free vibration of functionally graded carbon nanotube reinforced composite cylindrical panels. *Composite Structures*, 142, 45-56. https://doi.org/10.1016/j.compstruct.2015.12.071

[6] Y. Kiani. (2017). Dynamics of FG-CNT reinforced composite cylindrical panel subjected to moving load. *Thin-Walled Structures*, 111, 48-57. https://doi.org/10.1016/j.tws.2016.11.011

[7] C. Li, C. Zhu, C.W. Lim, S. Li. (2022). Nonlinear in-plane thermal buckling of rotationally restrained functionally graded carbon nanotube reinforced composite shallow arches under uniform radial loading. *Applied Mathematics and Mechanics*, 43, 1821-1840. https://doi.org/10.1016/j.apm.2019.01.024

[8] A. Alibeigloo. (2016). Thermoelastic analysis of functionally graded carbon nanotube reinforced composite cylindrical panel embedded in piezoelectric sensor and actuator layers. *Composites Part B: Engineering*, 98, 225-243. https://doi.org/10.1016/j.compositesb.2016.05.010

[9] K.M. Liew, A. Alibeigloo. (2021). Predicting bucking and vibration behaviors of functionally graded carbon nanotube reinforced composite cylindrical panels with three-dimensional

flexibilities. *Composite Structures*, 256, 113039. https://doi.org/10.1016/j.compstruct.2020.113039

[10] E.G. Macías, L.R. Tembleque, R.C. Triguero, A. Sáez. (2017). Buckling analysis of functionally graded carbon nanotube-reinforced curved panels under axial compression and shear. *Composites Part B: Engineering*, 108, 243-256. https://doi.org/10.1016/j.compositesb.2016.10.002

[11] V. Bhagat, P. Jeyaraj, S.M. Murigendrappa. (2018). Buckling and Free Vibration Behavior of a Temperature Dependent FG-CNTRC Cylindrical Panel Under Thermal Load. *Materials Today: Proceedings*, 5(11), 23682-23691. https://doi.org/10.1016/j.matpr.2018.10.158

[12] H.S. Shen, Y. Xiang, F. Lin. (2017). Nonlinear bending of functionally graded graphene-reinforced composite laminated plates resting on elastic foundations in thermal environments. *Composite Structures*, 170, 80-90.https://doi.org/10.1016/j.compstruct.2017.03.001

[13] H.S. Shen, Y. Xiang, F. Lin, D. Hui. (2017). Buckling and postbuckling of functionally graded graphene-reinforced composite laminated plates in thermal environments. *Composites Part B: Engineering*, 119, 67-78. https://doi.org/10.1016/j.compositesb.2017.03.020

[14] H.S. Shen, Y. Xiang, F. Lin. (2017). Nonlinear vibration of functionally graded graphene-reinforced composite laminated plates in thermal environments. *Computer Methods in Applied Mechanics and Engineering*, 319, 175-193. https://doi.org/10.1016/j.cma.2017.02.029

[15] H.S. Shen, Y. Xiang, Y. Fan. (2019). Vibration of thermally postbuckled FG-GRC laminated plates resting on elastic foundations. *Journal of Vibration and Control*, 25(9), 1507-1520. https://doi.org/10.1016/j.compstruct.2016.08.040

[16] H.S. Shen, Y. Xiang, Y. Fan, D. Hui. (2018). Nonlinear vibration of functionally graded graphene-reinforced composite laminated cylindrical panels resting on elastic foundations in thermal environments. *Composites Part B: Engineering*, 136, 177-186. https://doi.org/10.1016/j.compositesb.2017.10.032

[17] M. Mirzaei, Y. Kiani. (2017). Isogeometric thermal buckling analysis of temperature dependent FG graphene reinforced laminated plates using NURBS formulation. *Composite Structures*, 180, 606-616. https://doi.org/10.1016/j.compstruct.2017.08.057

[18] Y. Kiani. (2018). NURBS-based isogeometric thermal postbuckling analysis of temperature dependent graphene reinforced composite laminated plates. *Thin-Walled Structures*, 125, 211-219. https://doi.org/10.1016/j.tws.2018.01.024

[19] Y. Kiani. (2018). Isogeometric large amplitude free vibration of graphene reinforced laminated plates in thermal environment using NURBS formulation. *Computer Methods in Applied Mechanics and Engineering*, 332, 86-101. https://doi.org/10.1016/j.cma.2017.12.015

[20] F. Abbaspour, H. Arvin, Y. Kiani. (2022). Mechanical buckling analysis of functionally graded composite laminated plates reinforced with temperature dependent graphene sheets resting on elastic foundation. *ZAMM - Journal of Applied Mathematics and Mechanics*, 102(1), e202100097. https://doi.org/10.1002/zamm.202100097

[21] Y. Zheng, Y. Wang, J. Huang, Z. Tan. (2024). Flutter stability analysis of composite corrugated plates in supersonic flow. *Archive of Applied Mechanics*, 94, 1079-1098.

https://doi.org/10.1007/s00419-024-02568-8

[22] S. Pathirana, P. Qiao. (2020). Elastic local buckling of periodic sinusoidal corrugated composite panels subjected to in-plane shear. *Thin-Walled Structures*, 157, 107134. https://doi.org/10.1016/j.tws.2020.107134

[23] S. Pathirana, P. Qiao. (2019). Local buckling analysis of periodic sinusoidal corrugated composite panels under uniaxial compression. *Composite Structures*, 220, 148-157. https://doi.org/10.1016/j.compstruct.2019.03.050

[24] N.T. Phuong, N.T. Trung, T.D. Kien, H.D. Tuan, V.H. Nam. (2021). Nonlinear vibration of full-filled fluid corrugated sandwich functionally graded cylindrical shells. *Journal of Vibration and Control*, 27(9-10), 1020-1035. https://doi.org/10.1177/1077546320936537

[25] Y. Xia, M.I. Friswell, E.I. Saavedra Flores. (2012). Equivalent models of corrugated panels. *International Journal of Solids and Structures*, 49(13), 1453-1462. https://doi.org/10.1016/j.ijsolstr.2012.02.023

[26] D.T.K. My, V.M. Duc, N.H. Giang, N.T. Phuong, V.H. Nam. (2024). Buckling and Postbuckling of Laterally Pressured Sandwich FG-GRC Laminated Toroidal Shell Segments with Corrugated Core in Thermal Environment. *International Journal of Structural Stability and Dynamics*, 24(04), 2450036. https://www.worldscientific.com/doi/epdf/10.1142/S0219455424500366

[27] V.H. Nam, L.N. Ly, D.T.K. My, V.M. Duc, N.T. Phuong. (2024). On the nonlinear buckling and postbuckling responses of sandwich FG-GRC toroidal shell segments with corrugated core under axial tension and compression in the thermal environment. *Polymer Composites*, 45(15), 13737-13752. https://doi.org/10.1002/pc.28732

[28] D.T. Dong, D.T.K. My, V.M. Duc, L.N. Ly, V.T. Hung, V.H. Nam. (2024). Nonlinear torsional buckling of corrugated core sandwich toroidal shell segments with graphene-reinforced coatings in temperature change using the Ritz energy method. *Applied Mathematical Modelling*, 126, 739-752. https://doi.org/10.1016/j.apm.2023.11.027

[29] V.M. Duc, D.T.K. My, V.H. Nam. (2024). Nonlinear buckling and postbuckling of FG-CNTRC sandwich plates with multi-layer corrugated FG-CNTRC core. *Journal of Science and Transport Technology*, 4(4), 55-70. https://doi.org/10.58845/jstt.utt.2024.en.4.4.55-70

[30] V.H. Nam, L.N. Ly, D.T.K. My, N.T. Phuong, (2025). An analytical approach for nonlinear global buckling behavior of sandwich cylindrical panels with multilayer corrugated CNT-reinforced core in thermal environment, *Engineering Structures*, 345, Part B, 121570. https://doi.org/10.1016/j.engstruct.2025.121570

[31] H.S. Shen, Y. Xiang, Y. Fan. (2018). Postbuckling of functionally graded graphene-reinforced composite laminated cylindrical panels under axial compression in thermal environments. *International Journal of Mechanical Sciences*, 135, 398-409. https://doi.org/10.1016/j.ijmecsci.2017.11.031

[32] P.T. Thang, T.T. Nguyen, J. Lee. (2016). Nonlinear static analysis of thin curved panels with FG coatings under combined axial compression and external pressure. *Thin-Walled Structures*, 107, 405-414. https://doi.org/10.1016/j.tws.2016.06.0